Scientific Contributions Oil & Gas, Vol. 48. No. 2, August: 217 - 237

SCIENTIFIC CONTRIBUTIONS OIL AND GAS
Testing Center for Oil and Gas
LEMIGAS

Journal Homepage:http://www.journal.lemigas.esdm.go.id
ISSN: 2089-3361, e-ISSN: 2541-0520

The Use of Modified Rock Physics Template to Monitor Fluid Saturation in Carbonate Reservoir

Riskiray Ryannugroho[1,2], Sonny Winardhi[1,2], Djoko Santoso[1,2], Mohammad Rachmat Sule[1,2], Krishna Agra Pranatikta[1], Fernando Lawrens Hutapea[1,2], and Dona Sita Ambarsari[1,2].

[1]Geophysical Engineering Study Program, Faculty of Mining and Petroleum Engineering, Institut Teknologi Bandung
Ganesha Street No.10, Lebak Siliwangi Coblong, Bandung, West Java 40132, Indonesia.

[2]Center for CO_2 and Flared Gas Utilization, Institut Teknologi Bandung
Ganesha Street No.10, Lebak Siliwangi Coblong, Bandung, West Java 40132, Indonesia.

Corresponding author: riskiray.r@gmail.com

Manuscript received: April 24th, 2025; Revised: May 19th, 2025
Approved: May 22th, 2025; Available online: May 23th, 2025; Published: May 27th, 2025.

ABSTRACT - Rock physics template (RPT) is defined as a crossplot of acoustic impedance (AI) against the ratio of P- and S-wave velocities that is used for lithology and pore-fluid interpretation of well log data and/or pre-stack seismic inversion results. This study is employing an interactive RPT approach, which facilitates calibration using available data and enhances the interpretation and prediction of pore fluids within carbonate reservoir rocks. A previously established RPT model is modified to construct the rock physics template and to interpret trends in porosity and fluid saturation within a predictive framework. The modified approach to the RPT formulation demonstrates that the proposed model yields more accurate porosity and fluid saturation trends for the reservoir rocks in the study area than the previous RPT model, as evidenced by the theoretical curves in the Rock Physics Template (RPT) domain. To predict fluid saturation, a workflow is developed to build the modified RPT model that incorporates the Curved Pseudo Elastic Impedance (CPEI) and the Pseudo Elastic Inversion for Lithology (PEIL) attributes. These attributes are used to regulate the fluid saturation and density values in the model space and to assist in constructing the RPT model. The proposed method is also applied to monitor fluid saturation changes in oil, gas, or CO_2 cases, utilizing the Vp/Vs ratio and acoustic impedance derived from the seismic inversion data, and allows calibration with available datasets such as well logs and cores.

Keywords: rock physics template, carbonate reservoir, porosity, fluid saturation.

How to cite this article:

Riskiray Ryannugroho, Sonny Winardhi, Djoko Santoso, Mohammad Rachmat Sule, Krishna Agra Pranatikta, Fernando Lawrens Hutapea, and Dona Sita Ambarsari, 2025, The Use of Modified Rock Physics Template to Monitor Fluid Saturation in Carbonate Reservoir, Scientific Contributions Oil and Gas, 48 (2) pp. 217-237. DOI org/10.29017/scog.v48i2.1749.

INTRODUCTION

Accurate interpretation of fluid saturation in the subsurface is essential for hydrocarbon field development and for monitoring CO_2 storage operations. In the context of carbon capture and storage (CCS) monitoring, fluid saturation is a critical parameter for verifying CO_2 plume migration, quantifying stored volumes, and ensuring long-term containment (IPCC 2005). Moreover, accurate saturation mapping also supports model validation and updating, improving the reliability of reservoir simulations (Crain et al. 2024; Pelemo-Daniels et al. 2023).

Achieving these monitoring goals requires a robust link between fluid saturation and the elastic properties of the reservoir, as captured through rock physics relationships. Estimating fluid saturation from elastic properties remains challenging due to the nonlinear and often non-unique relationship between rock elastic properties, porosity, and fluid composition. The RPT has been widely adopted as a practical and intuitive method for interpreting seismic or well log data in terms of lithology, pore structure and/or fluid variation (Avseth & Odegaard 2004; Hutami et al. 2019). However, the available RPT often requires extensive modeling and laboratory data to accurately model reservoir specific conditions.

In this study, the RPT framework proposed by Fawad & Mondol (2022) was utilized to address the need for a practical yet robust method for fluid interpretation under conditions of limited subsurface data, which typically consist only of conventional well logs. However, that RPT model does not adequately capture the relationship between rock porosity and fluid saturation partly due to simplified assumptions. To overcome this limitation, the model was modified to more accurately represent the relationship between porosity and saturation within the RPT crossplot domain. This was done by incorporating Gassmann (1951) assumption. The modified RPT was then used to interpret and estimate fluid saturation from available well data in the Gundih area of Central Java, in anticipation of planned CO_2 storage and Enhanced Gas Recovery (EGR) targeting the Kujung Formation (Aziz et al. 2023; Sule et al. 2019).

METHODOLOGY

Rock physics template

RPT is a tool that integrates rock physics models, well log data, and seismic attributes to establish relationships between elastic properties, such as velocity, density, and impedance; and reservoir parameters such as porosity, lithology, and fluid saturation. RPTs are used to visualize the behavior of rocks and pore fluids within an elastic property space; typically the *Vp/Vs* ratio versus acoustic impedance, thereby facilitating the interpretation of subsurface formations in terms of lithology, porosity, and fluid content (Avseth & Odegaard 2004). By applying theoretical models, such as Gassmann's (1951) equation for fluid substitution and the Hertz-Mindlin model (1949) for granular media, RPT is often used to predict rock and fluid properties, thereby enhancing reservoir characterization and hydrocarbon exploration.

Building an RPT involves selecting appropriate rock physics models based on the reservoir type, collecting well log data, such as porosity, velocity, and density logs, and plotting these data in cross-plots of the elastic properties (Figure 1). Theoretical rock physics trends are then overlaid onto these plots to create a predictive framework. Calibration is a critical step in which the RPT is refined, using core samples, well log correlations, and laboratory measurements to ensure that the modeled trends align with real data observations. This process enhances the accuracy of seismic interpretations by ensuring that the RPT represents the actual subsurface conditions.

In addition, RPTs are specific to sites and consider local geological conditions (Avseth et al. 2010). The geological limitations of rock physics models include lithology, mineral composition, burial depth, diagenesis, pressure, and temperature. Specifically, it is vital to incorporate only the anticipated lithologies, as a siliciclastic system will feature different lithofacies than a carbonate system. A rock physics template (RPT) in the *Vp/Vs* versus AI cross-plot domain incorporates rock physics models that are locally constrained by depth (i.e., pressure), mineral composition, critical porosity, and fluid characteristics. The arrows and color-coded lines in the RPT illustration (Figure 1) conceptually represent the following geological trends: 1) increasing shaliness, 2) increasing gas saturation, 3) increasing effective pressure, and 4) increasing porosity.

The trends captured by the RPT also allow for the identification of phenomena induced by CO_2 injections, particularly in carbonate-rich reservoirs. One such phenomenon is the dissolution of carbonate minerals, which can occur due to the acidification of formation brine when CO_2 dissolves and forms carbonic acid. This geochemical reaction increases rock porosity by dissolving calcite or dolomite along pore walls and fractures (Aziz et al. 2025; Gaus 2010; Luquot & Gouze 2009). As a result, changes in porosity lead to alterations in the elastic properties and fluid saturation distribution, both of which can be reflected in the RPT domain.

between Wyllie's time average and the bulk density is as follows:

$$\frac{AI(1-\phi)}{V_{p_{ma}}} + \frac{AIS_{fl}\phi}{V_{p_{fl}}} + \frac{AI(1-S_{fl})\phi}{V_{p_w}} = (1-\phi)\rho_{ma} + S_{fl}\phi\rho_{fl} + (1-S_{fl})\phi\rho_w \quad (1)$$

where *AI* denotes the acoustic impedance which comprises the compressional velocity of the rock multiplied by its bulk density, Vpma is the compressional velocity of rock grain, Vpfl is the compressional velocity of fluid other than

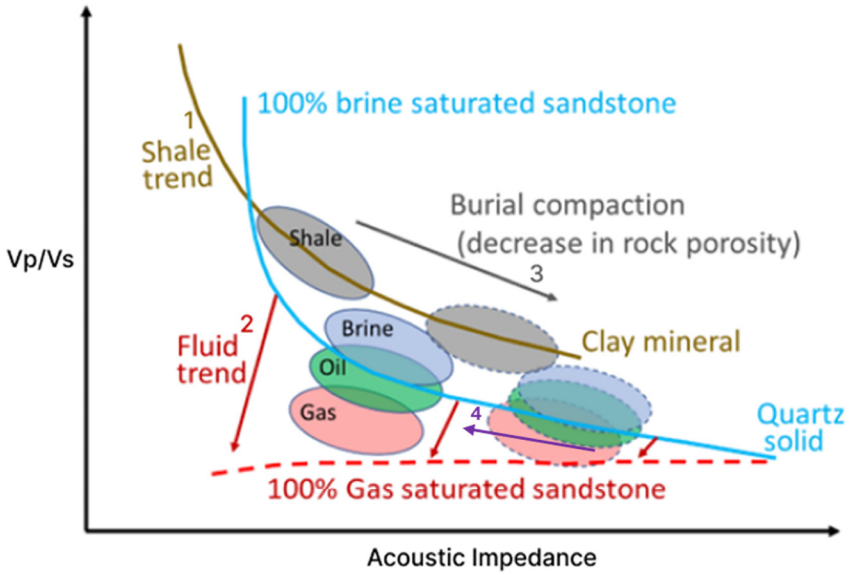

Figure 1. Typical rock physics template for sandstone reservoir (adapted from Avseth et al. (2010)). The lithology, fluid, shale, and burial compaction trends can be observed through the AI vs Vp/Vs crossplot framework (Avseth & Odegaard 2004)

Fawad-mondol RPT (FM-RPT)

Fawad & Mondol (2022) developed an approach to building an RPT model that is straightforward, adaptable, and robust. This model can be developed without modeling at the level of rock moduli, such as the Hertz-Mindlin model (Mindlin 1949) and the modeling Hashin-Shtrikman bounds (Hashin & Shtrikman 1963), yet it allows for flexible application to fit the RPT model based on the data utilized.

In their study, Fawad and Mondol employed a new approach based on rock physical properties to detect changes in CO_2 saturation inside the siliciclastic storage reservoir due to CO_2 injection. They utilized Wyllie's Time Average equation (Wyllie et al. 1956), the bulk density equation, and the compressional to shear velocity ratio *(Vp/Vs)* from Lee et al. (1996) to develop an RPT model that aligns with data observations. The relationship

formation water; e.g., oil, gas, CO2, etc, Vpw is the compressional velocity of formation water/brine, ϕ is the rock porosity, and Sfl is the fluid saturation other than formation water, ρ_ma is the rock matrix density, ρ_fl is the density of fluid other than formation water; e.g., oil, gas, CO2, etc, and ρ_w is the water/brine velocity. The *Vp/Vs* ratio relationship proposed by Lee et al. (1996) was used to link the developed equation with the relationship between

$$\frac{Vp}{Vs} = \frac{1}{[G\alpha(1-\phi)^N]} \quad (2)$$

the S-wave and P-wave velocities:

where *Vp* and *Vs* are compressional and shear wave velocities, respectively; denotes the rock porosity, and is the mineral/rock grain *Vs/Vp* ratio

defined matrix-mineral pole on the RPT plane. *G* and *N* are variables that allow the RPT curve to be calibrated and fitted to available data. *G* is a variable that enables vertical adjustment of the rock matrix pole (rock matrix *Vp/Vs* point); whereas, *N* controls the curvature of the fluid saturation line, which corresponds to the degree of compaction/ shale content. By integrating equations (1) and (2), the relationship for predicting fluid saturation (Sfl) can be rewritten as:

$$S_{fl} = \frac{\left\{\begin{array}{l} \rho_{ma} + \left[1 - \left(\frac{V_S}{V_p G\alpha}\right)^{\frac{1}{N}}\right](\rho_w - \rho_{ma}) \\ - AI\left[\frac{1}{V_{p_{ma}}} + \left(1 - \left(\frac{V_S}{V_p G\alpha}\right)^{\frac{1}{N}}\right)\left(\frac{1}{V_{p_w}} - \frac{1}{V_{p_{ma}}}\right)\right] \end{array}\right\}}{\left\{\left[1 - \left(\frac{V_S}{V_p G\alpha}\right)^{\frac{1}{N}}\right]\left[AI\left(\frac{1}{V_{p_{fl}}} - \frac{1}{V_{p_w}}\right) - (\rho_{fl} - \rho_w)\right]\right\}} \quad (3)$$

S_{fl} in Equation (3) is the fluid saturation in the rock pore space other than the formation water (brine), which can be oil, gas, or CO_2.

Modified fawad-mondol RPT (MFM-RPT)

The equation for the velocity ratio *Vp/Vs* formulated by Lee et al. (1996) in equation (2) shows that the P-wave and S-wave velocity ratio depends solely on porosity, although it should also account for the fluid saturation effect. To accommodate this assumption, we modified the *Vp/Vs* ratio equation proposed by Lee et al. (1996) and incorporated into the FM-RPT model. Our approach is based on the Gassmann (1951) assumptions, in which rock with the same matrix and porosity have shear modulus value that is not affected by pore fluid, which can be expressed as follows:

$$\mu_{sat} = \mu_{dry} \quad (4)$$

with is the shear modulus of saturated rock, and *μsat* is the shear modulus of dry rock. Thus, the relationship between the shear wave velocity of the rock under saturated and dry conditions can be explained as follows:

$$V_{s_{sat}} = \sqrt{\frac{\rho_{dry}}{\rho_{sat}}}\, V_{s_{dry}} \quad (5)$$

with as the shear velocity of rock in saturated condition, as the shear velocity of rock in dry condition. the dry rock density, and the density of rock in a saturated condition. The above equation represents a modification of the compressional and shear wave ratio equation developed by Lee et al. (1996) that integrates the assumption of Gassmann (1951). In this relationship, the presence of porosity and fluid saturation is reflected in the variable ρ_{sat}, which indicates that the modification produces a relationship between velocity Vs_{sat} as a function of rock porosity and fluid saturation. The variable Vs_{dry} can be approximated using empirical equations developed by Phani & Niyogi (1986):

$$V_{s_{dry}} = (1-\phi)^N V_{s_{ma}} \quad (6)$$

This equation expresses the relationship between Vs_{ma} as the mineral/rock grain S-wave velocity, and the fitting parameter (*N*), which denotes the degree of compaction. To accommodate the calibration function and fit to the observed data, we can rewrite the Vs_{ma} parameter as a function of Vp_{ma} and *G* parameters using the relationship in in Equation (2) as follows:

$$V_{s_{ma}} = G\,\alpha\,V_{p_{ma}} \quad (7)$$

The relationship between rock density in a dry state, rock mineral/matrix density, and rock porosity can be expressed using the following equation:

$$\rho_{dry} = (1-\phi)\rho_{ma} \quad (8) \quad (8)$$

After defining Equations (6), (7), and (8), the variables are substituted in Equation (5), which is expressed as follows:

$$V_{s_{sat}} = \sqrt{\frac{(1-\phi)\rho_{ma}}{\rho_{sat}}}\left[(1-\phi)^N G\alpha V_{p_{ma}}\right] \quad (9)$$

The above equation is a modified equation that incorporates the Gassmann (1951) assumption. The *G* and *N* parameters also act as interrelated flexibility elements to accommodate calibration to observed data. This modification also produces a new form of the porosity equation, which can be rewritten from Equation (6) as follows:

$$\phi = 1 - \left(\frac{V_{s_{sat}}^2 \rho_{sat}}{G^2\alpha^2 V_{p_{ma}}^2 \rho_{ma}}\right)^{\frac{1}{2N+1}} \quad (10)$$

By relating the modified porosity equation in Equation (10) to the porosity equation between the Wyllie Time average relationship and bulk density in Equation (1), we obtained a modified relationship to predict rock fluid saturation, using the following expression:

$$S_{fl} = \frac{\left\{ \rho_{ma} + \left[1 - \left(\frac{V_{s_{sat}}^2 \rho_{sat}}{G^2 \alpha^2 V_{p_{ma}}^2 \rho_{ma}} \right)^{\frac{1}{2N+1}} \right] (\rho_w - \rho_{ma}) \right\}}{\left\{ -AI \left[\frac{1}{V_{p_{ma}}} + \left(1 - \left(\frac{V_{s_{sat}}^2 \rho_{sat}}{G^2 \alpha^2 V_{p_{ma}}^2 \rho_{ma}} \right)^{\frac{1}{2N+1}} \right) \left(\frac{1}{V_{p_w}} - \frac{1}{V_{p_{ma}}} \right) \right] \right\}} \quad (11)$$

$$\left\{ \left[1 - \left(\frac{V_{s_{sat}}^2 \rho_{sat}}{G^2 \alpha^2 V_{p_{ma}}^2 \rho_{ma}} \right)^{\frac{1}{2N+1}} \right] \left[AI \left(\frac{1}{V_{p_{fl}}} - \frac{1}{V_{p_w}} \right) - (\rho_{fl} - \rho_w) \right] \right\}$$

Equation (11) demonstrates a novel approach for predicting fluid saturation where the modified RPT model incorporates an equation that accounts not only for porosity change (Equation 2) but also accommodates variations in fluid saturation by introducing into the equation. The model also shows the ability to monitor fluid saturation directly from seismic data by employing the acoustic impedance inversion, and/or incorporating simultaneous inversion results to obtain the Vs properties and utilize the PEIL attribute to approach the ρ_{sat} .

CPEI and PEIL attributes

Curved Pseudo Elastic Impedance (CPEI) is an attribute that aims to approach the function of the nonlinear curve equation of RPTs. Avseth et al. (2014) first introduced CPEI as an attribute that is sensitive to fluid saturation. The original equation is defined as a function of the deviation from the nonlinear wet sandstone curve in the AI-*Vp/Vs* ratio domain and is used to show the sensitivity of CPEI to fluid saturation. The CPEI attribute equation based on Avseth et al. (2014) uses an approach to the particular RPT's curve through a polynomial or logarithmic function as a function of the AI-*Vp/Vs* ratio.

Besides the CPEI attribute, which is sensitive to fluid saturation, there is another attribute that relates to the degree of rock compaction, known as Pseudo-Elastic Impedance for Lithology (PEIL). PEIL indicates the deviation from a straight line parallel to the shear modulus constant. The building of the PEIL attribute uses the shear modulus trend as a reference and is capable of illustrating the direction of density and porosity changes.

The CPEI and PEIL attributes have been extensively developed so that they can be accommodated and calibrated for different geological and reservoir conditions. Palgunadi et al. (2016) simplified the equation by using the trigonometric function, enabling simple attributes rotation through the axes. Winardhi et al. (2023) modified the equation by adding exponents *m* and *n* to increase the flexibility of the CPEI and PEIL trends in directing their curves to approximate the curvilinear trend of the RPT model (Figure 2). The trigonometric equations for CPEI and PEIL that were proposed by Winardhi et al. (2023) are defined as follows:

$$CPEI = AI^n \left(V_p / V_s \right)^m \cos \chi + AI^n \left(V_s / V_p \right)^m \sin \chi \quad (12)$$

$$PEIL = -AI^n \left(V_p / V_s \right)^m \sin \chi + AI^n \left(V_s / V_p \right)^m \cos \chi \quad (13)$$

CPEI and PEIL attributes were utilized in this study to regularize the fluid saturation and density values in the model space, assisting in the building and calibration of the proposed RPT model.

Warm colors indicate a high attribute value, whereas cooler colors indicate a low value. The top panel shows the adaptability in directing the curvilinear CPEI attribute using *m, n, and chi* parameters to imitate the water saturation trend changes in the RPT space, while the bottom panel shows the flexibility of the PEIL attribute to approach the density or porosity trend.

The modified equations were used to build the RPT model, produce the theoretical curve, and estimate the rock fluid saturation. First, the theoretical RPT curve was built to observe and analyze the relationship between the rock physical properties (water saturation and porosity) and elastic properties on the AI and *Vp/Vs* space. The model space was defined using hypothetically rock porosity values, ranging from 0 to 0.3, based on the assumption that the critical porosity of limestone is 0.3. Water saturation was assumed to range from 0 to 1, representing a transition from fully water-saturated to fully oil, gas, or CO_2 saturated rock. Using these parameters, the corresponding elastic properties, the acoustic impedance (AI) and *Vp/Vs* ratio were derived and plotted in the RPT space. This approach enabled the observation of relationships between rock petrophysical properties and elastic responses as described by the FM-RPT and MFM-RPT models.

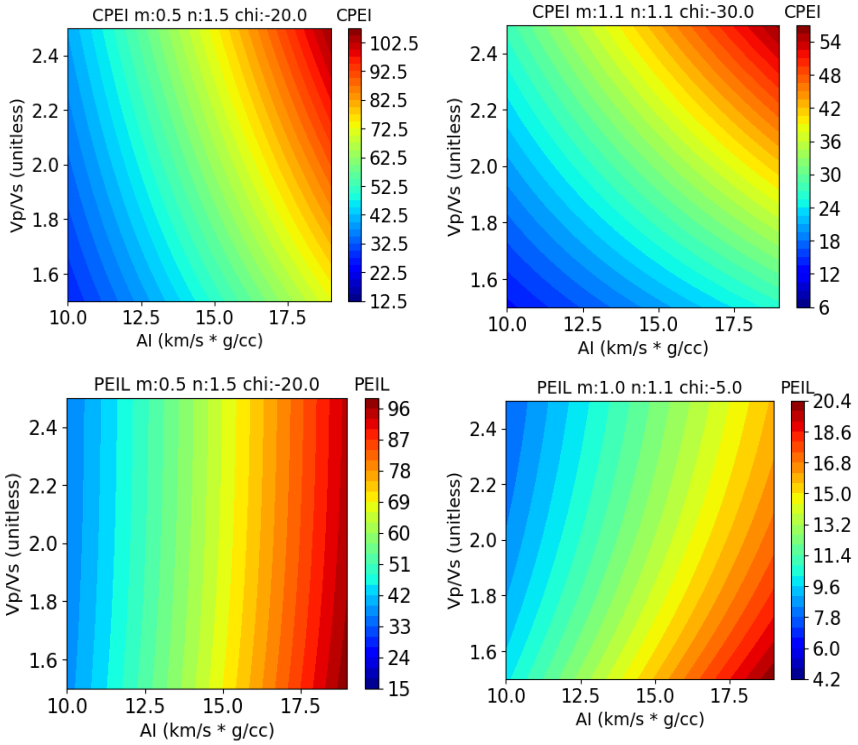

Figure 2. The influence of *m, n and chi,* on the CPEI and PEIL curve to meet the rock physics template (RPT).

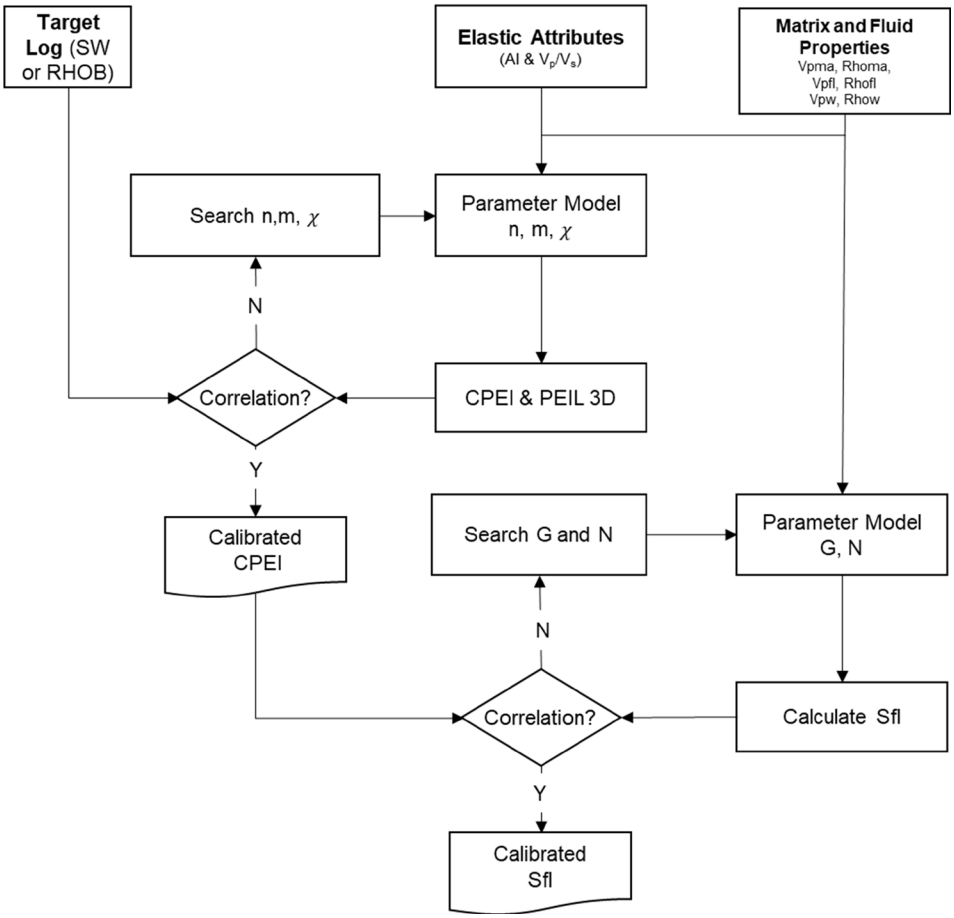

Figure 3. Workflow to predict the fluid/water saturation of reservoir rock. The inputs required are the velocity and density of the rock matrix and fluids. The CPEI and PEIL attributes are used as regularizations to search for the G and N parameters.

A workflow is proposed to predict fluid saturation using the modified equation (Figure 3), and is described as follows: 1). Prepare well data of *Vp*, *Vs* and density logs and petrophysical interpretation log results, such as porosity and water saturation and/or core data, if available; 2). Create CPEI attributes using *m*, *n*, and values within a certain range, using a grid search algorithm and calculating the cross-correlation coefficient value between CPEI values for each *m*, *n*, and value and water saturation logs. 3). Cut off the CPEI values to imitate the water saturation distribution pattern and perform scaling according to water saturation logs. 4). The scaled CPEI attribute with the highest cross-correlation value to the observed water saturation log is then obtained. The calibrated CPEI attribute is used as the benchmark for fluid saturation prediction, as the water saturation value is regularized. 5). Calculate the fluid saturation, *Sfl* (1-S_W), using the modified equation for a specified range of *G* and *N* parameters using a grid-search algorithm. 6). Perform histogram matching between each of the *Sfl* predictions to the calibrated CPEI attribute and perform cross-correlation and misfit analyses between them. 7). Obtain the best prediction for the *Sfl* value with the highest cross-correlation coefficient and/or lowest misfit to the calibrated CPEI attribute. 8). Perform histogram matching between the best *Sfl* prediction value and 1-S_W logs and obtain the best corresponding prediction for fluid/water saturation.

The CPEI attribute is created based on Equation (14), where the process of fitting the variation of parameters *m*, *n*, and χ using the grid-search approach to the observed water saturation data (*SW*) is carried out until the best coefficient correlation is obtained. The CPEI attribute that best fits the water saturation data is then used as a proxy for *Sfl* prediction, creating a regularized water saturation value in the model space to assist in building the RPT model.

RESULTS AND DISCUSSION

Theoretical RPT curve

The RPT model developed by Fawad and Mondol (2021) utilizes the relationship between *Wyllie's Time Average* equation, bulk density, and velocity ratio (*Vp/Vs*) proposed by Lee et al. (1996), to produce a new approach for building an RPT model in the AI Vs. *Vp/Vs* domain. The main difference between the velocity ratio equation, which depends only on the porosity, and its modified model, which considers the effect of fluid saturation, can be observed in Figure 5. Variations of the AI and *Vp/Vs* scheme is displayed with different *color keys*; namely, porosity (ϕ), and fluid saturation ($S_{fl} = 1 - Sw$). The acoustic impedance (AI) was obtained as a function of the rock P-wave velocity and density; both were controlled by the porosity and fluid saturation factors.

The rock and fluid parameters used to build the RPT are listed in Table 1. The rock matrix compressional and shear wave velocities were estimated from the cross plot between the corresponding velocities and the rock porosity, and were determined by using linear approximation when the rock porosity was zero. The rock matrix density was also determined with the same method. The fluid density and velocity parameters were calculated using the Batzle & Wang (1992) equation, considering reservoir pressure and temperature.

The Fawad & Mondol (2022) RPT model, called FM-RPT, uses the relationship between Wyllie's Time Average, bulk density, and compressional and shear velocity ratio (*Vp/Vs*) to build a simple yet flexible RPT model. The ratio of *Vp/Vs* by Lee et al. (1996), which is stated in Equation (2), shows that the relationship between *Vp* and *Vs* is a function of the porosity only whereas it should account for fluid saturation. Thus, we used the modified function written in the Equation (9) so that the final equation to predict fluid saturation already considers Gassmann's assumption (Equation 11).

We created theoretical curves for both RPT models to determine how water saturation and rock porosity affect the AI value and *Vp/Vs* ratio in the model space (Figure 5). The right-hand end of both RPT models has the same point, where *Vp* and *Vs* and the density of rock matrixes exist; that is, where the rock is in a state where its porosity is equal to 0. The effect of fluid saturation can be recognized through the variation in curvature, which reflects the proportion of water and hydrocarbon fluids. The *Vp/Vs* ratio of FM-RPT, using Lee's original equation shows sensitivity to different porosities, but not to the water/fluid saturation variation. In other words, for a given constant porosity value and varying fluid saturation, the *Vp/Vs* ratio is uniform. This is considered inaccurate because the change in fluid saturation, assuming that the rock porosity does not change, should also influence the *Vp/Vs* ratio.

Parameter	Symbol	Value	Unit
Rock matrix P-wave Velocity	$V_{p\,ma}$	7.10	Km/s
Rock matrix S-wave Velocity	$V_{s\,ma}$	3.95	Km/s
Brine's P-wave Velocity	$V_{p\,w}$	1.51	Km/s
Oil's P-wave Velocity	$V_{p\,oil}$	1.08	g/cc
Gas P-wave Velocity	$V_{p\,gas}$	0.69	g/cc
Rock matrix density	ρ_{ma}	2.79	g/cc
Brine matrix	ρ_{w}	0.92	g/cc
Oil density	ρ_{oil}	0.79	g/cc
Gas (methane) density	ρ_{gas}	0.14	g/cc

Table 1
Properties used to build the RPT model

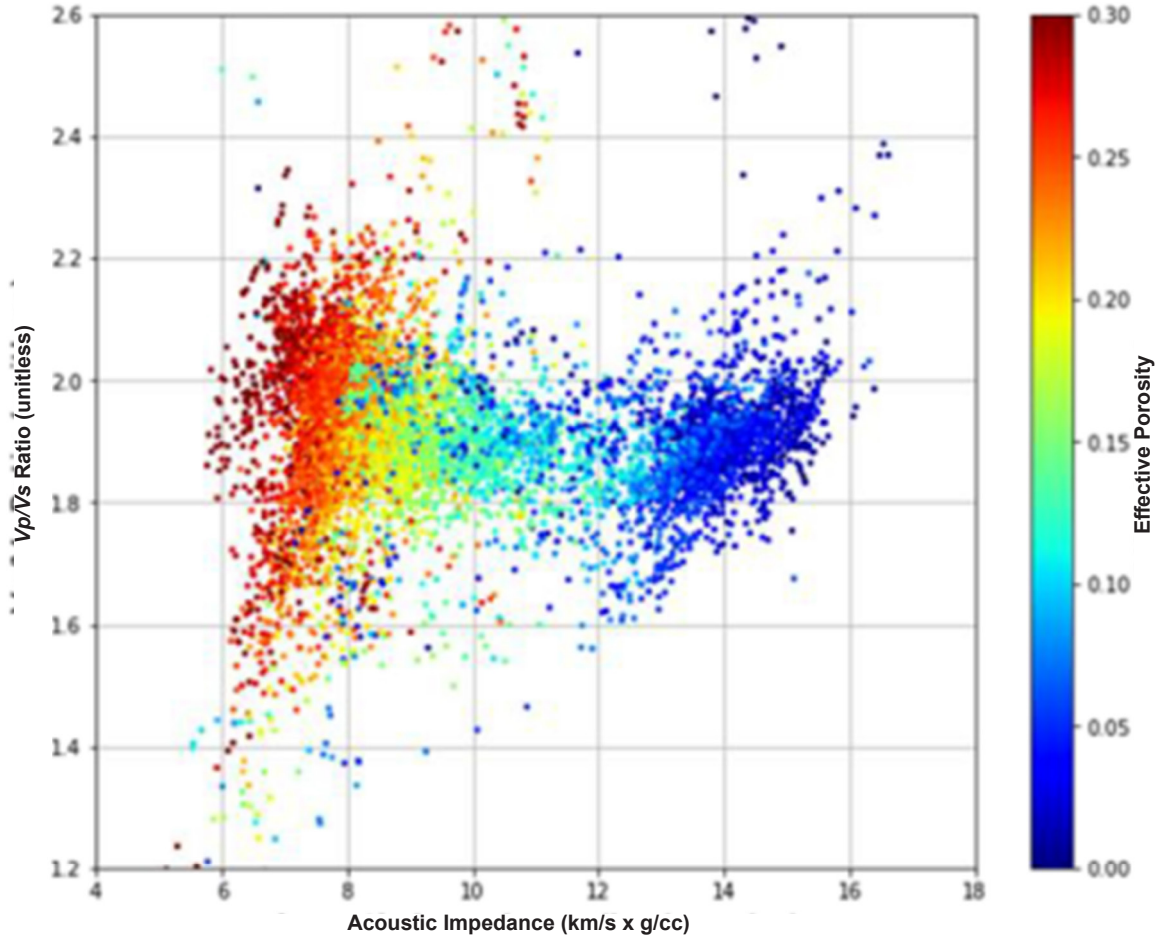

Figure 4. Cross-plot of the AI and *Vp/Vs* ratio of carbonate rocks in the East Java Basin with the color key illustrating effective porosity (Nugroho et al. 2023).

Meanwhile, the MFM-RPT using the modified Lee's *Vp/Vs* equation showed a better trend of porosity and fluid saturation. The porosity trend has more similarity to the AI and *Vp/Vs* ratio well log cross-plot of carbonate rock data in East Java based on a study report (Figure 4) and the conceptual trend in a typical RPT (Figure 1). Assuming that the rock porosity does not change, changes in rock water saturation should affect the *Vp/Vs* ratio. This observed trend in the theoretical curve indicates that the modified equation better accommodates the porosity and fluid saturation parameters in the RPT model space.

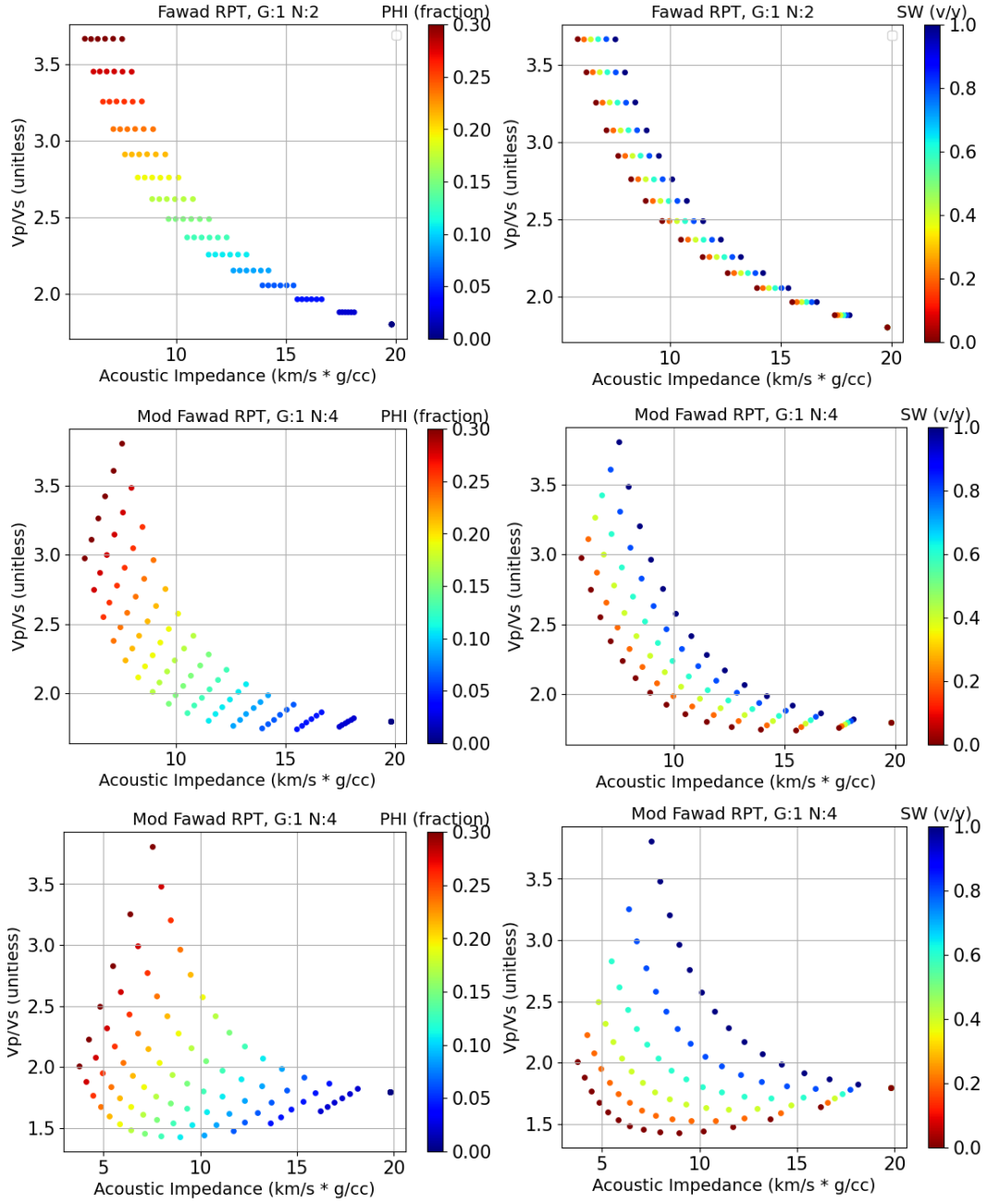

Figure 5. Theoretical curve of Rock Physics Template using the Fawad Model for oil-saturated scenario (a and b); the Modified Fawad Model for oil-saturated scenario (c and d); and for gas-saturated scenario (e and f). The theoretical RPT curve was constructed using the parameters given in Table 1. For the Fawad Model (FM-RPT), the *G* and *N* parameters used were 1 and 2, respectively. For the MFM-RPT, we used *G* and *N* parameters 1 and 4, respectively. The AI and Vp/Vs variation due to porosity (a, c and e) and water saturation (b, d, and f) changes show different trend between the Fawad Model (a - b) and the Modified Fawad Model (c – f). The MFM-RPT result give close resemblance to the porosity trend of East Java Basin RPT crossplot given in Figure 4

Prediction of fluid saturation

In this section, we discuss how the proposed method and workflow can be used to predict fluid saturation and calibrate well data. For this analysis, we used two available well(s) in the study area with relatively complete well log data (Figure 6) in the Kujung Formation intervals. In the study area, the Kujung Formation is a carbonate formation in the western margin of the East Cepu High that developed in several stages from the late Oligocene to Miocene periods, forming isolated platforms (Purwaningsih et al. 2002). Both wells penetrate the Kujung Formation interval, which consists of relatively clean, gas-bearing carbonate reservoir rocks with an average porosity of 10–15%. The interpreted depositional facies correspond to a platform-margin reef environment.

A CPEI attribute was created to regularize the water saturation distribution in the RPT model space. Using the grid-search approach, we found the most optimum CPEI parameter of *m*, *n*, and χ that best corresponds to water saturation log (S_W) for the KTB-02 well were 1, 2, and -40°, respectively, with a cross-correlation value of 0.78 (Figure **7**). We performed cut-off and scaling of the CPEI value to mimic the water saturation log. To predict density value in KTB-02 well (Figure 8), we performed the PEIL attribute and obtained the most optimum parameter of *m*, *n*, and χ, which are 1, 1 and -10° respectively. The cross-correlation value between the density log and PEIL attributes is 0.71 for the KTB-02 well.

For the RBT-02 well (Figures 9 and 10), The same analysis was performed and used to calibrate CPEI and PEIL for water saturations and density logs, respectively. The best CPEI attribute corresponding to the water saturation log was given by *m*, *n*, and χ of 1, 2.9, and -5° respectively, yielding a cross-correlation value of 0.68. Whereas, PEIL attribute is strongly correlate with the density log given by m, n, and χ parameter value of 1.1, 1, and -5.3° respectively, with a cross-correlation value of 0.75.

After the CPEI attribute was created, The attribute was used to assist in the estimation of fluid saturation for both wells. The CPEI attributes were employed to regularize the water saturation value within the AI and *Vp/Vs* ratio model space, thereby facilitating the search for optimal parameters. The results of fluid saturation estimation are seen in Figures 11 and 12. For the KTB-02 well, the optimum *G* and N parameters were 1.2 and 5.6 respectively. The cross-correlation between the estimated fluid saturation and 1-S_W log is 0.80. For the RBT-02 well, the most optimum *G* and *N* parameters were 1.16 and 6, respectively, with a cross- correlation value of 0.58 between the estimated fluid saturation and the 1-S_W log.

The results of the fluid saturation estimation using the proposed method were analyzed by superimposing the result with the water saturation log for the corresponding wells (Figure13). Generally, the predicted water saturation (1-*Sfl*) trend exhibited a similar pattern that aligned with the observed water saturation log. The accuracy of fluid saturation was quantified by the misfit using the root-mean-square error (RMSE) function. For the KTB-02 well, the cross-correlation and misfit to the observed water saturation log was 0.72 and 15.27, respectively. Whereas, for the RBT-02 well, the cross-correlation and misfit value for the fluid saturation, using the proposed model, was 0.59 and 35.75, respectively, in regard to the observed water saturation log. The relatively low correlation observed in RBT-02 compared to KTB-02 may be attributed to the higher volumetric clay content in the RBT-02 interval.

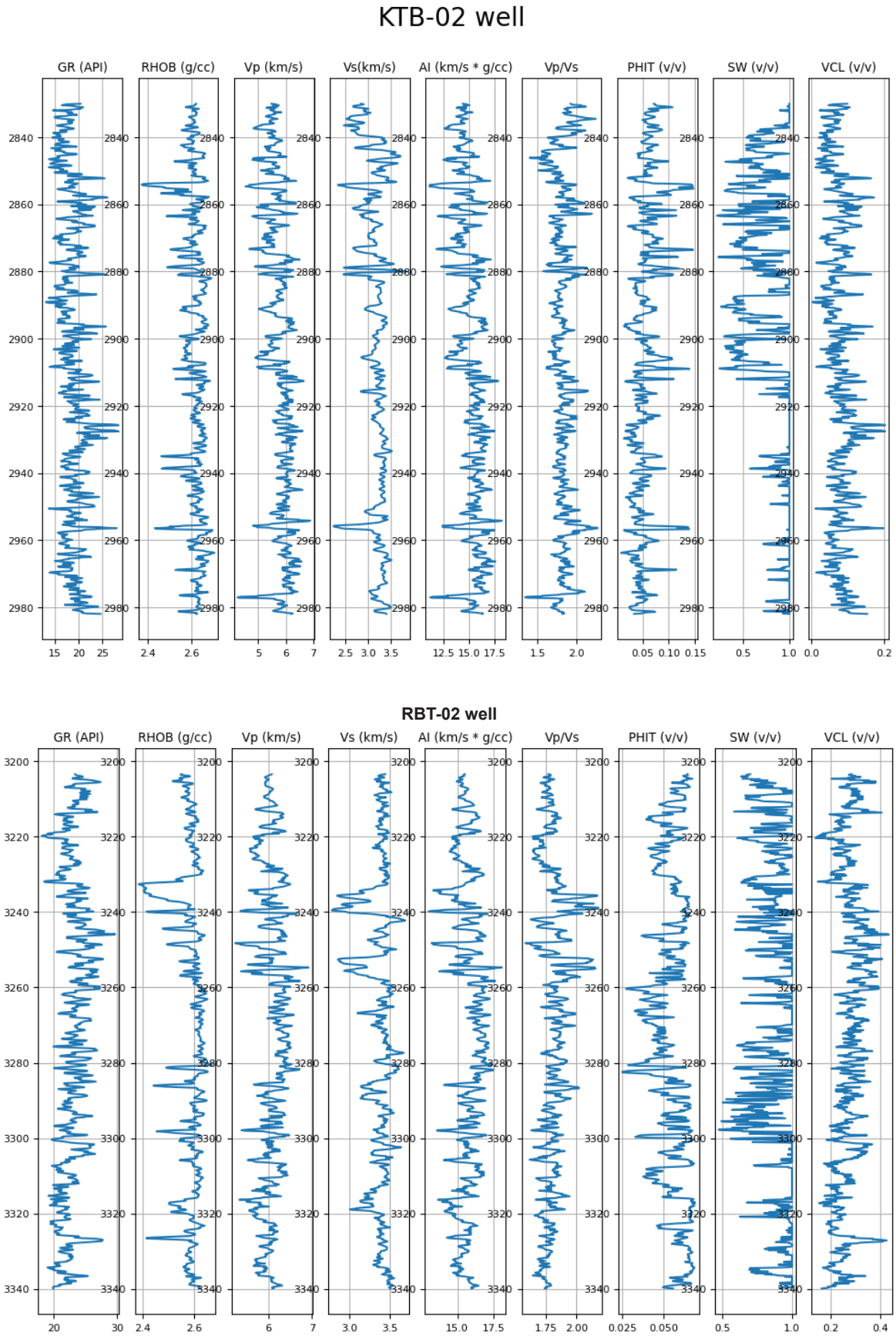

Figure 6. Available well data used in this analysis.

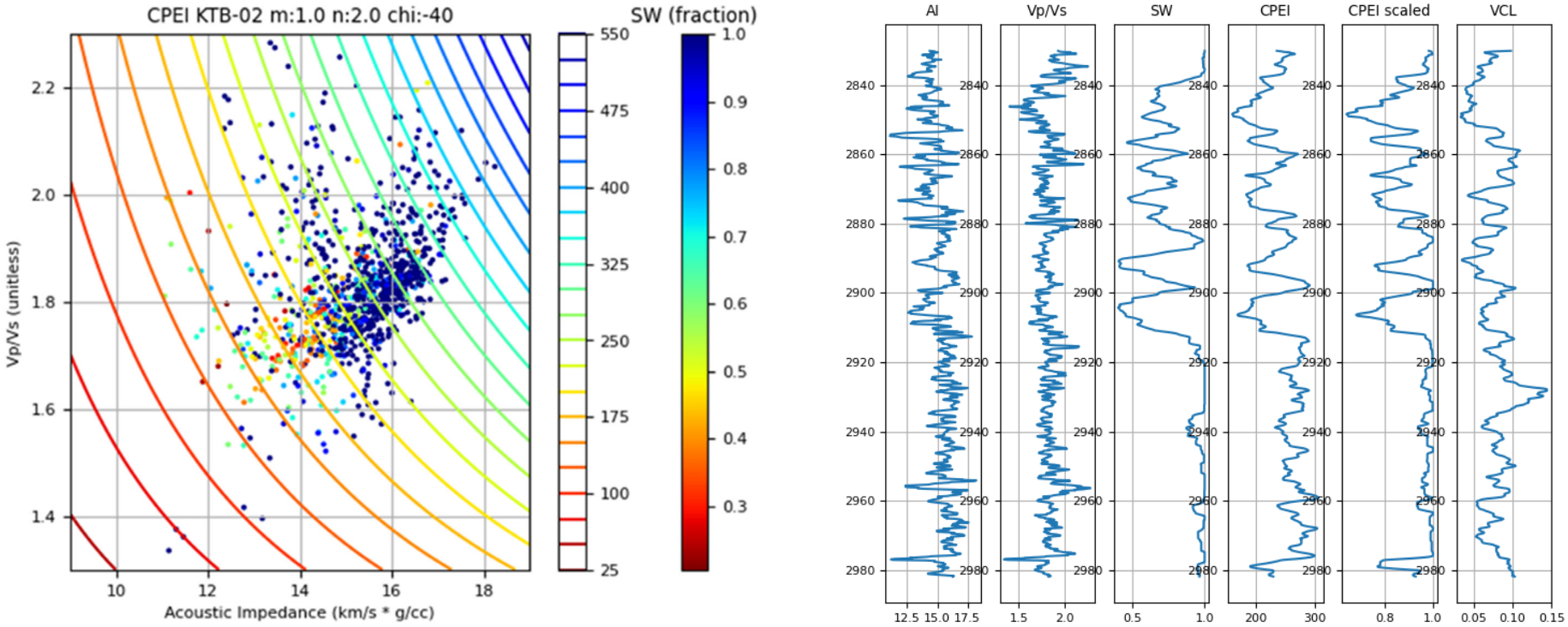

Figure 7. (Left) Calibrated CPEI attributes with respective well logs for the KTB-02 well. (Right) The CPEI-scaled attribute successfully approached the observed S_w log value.

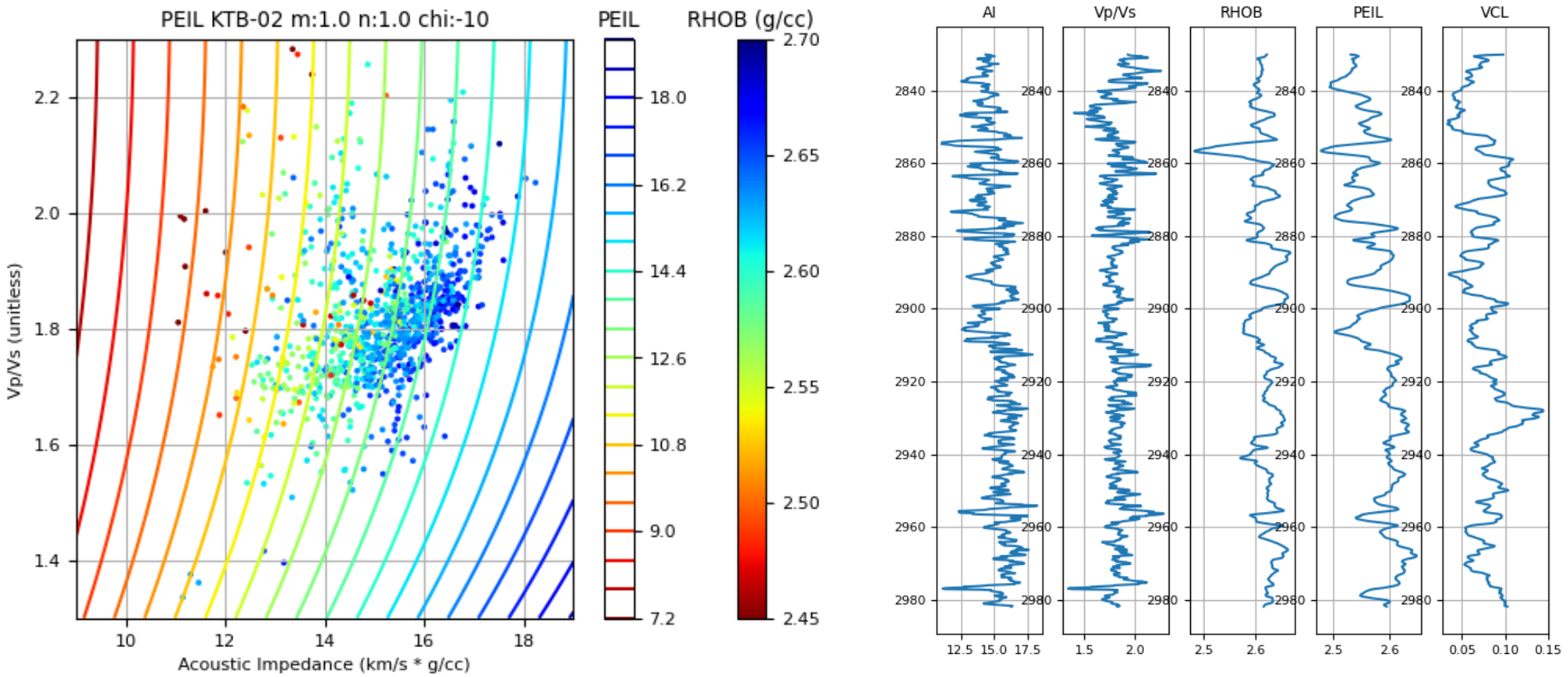

Figure 8. (Left) Calibrated PEIL attributes with respective well logs for the KTB-02 well. (Right) The PEIL attribute successfully approached the observed RHOB log value.

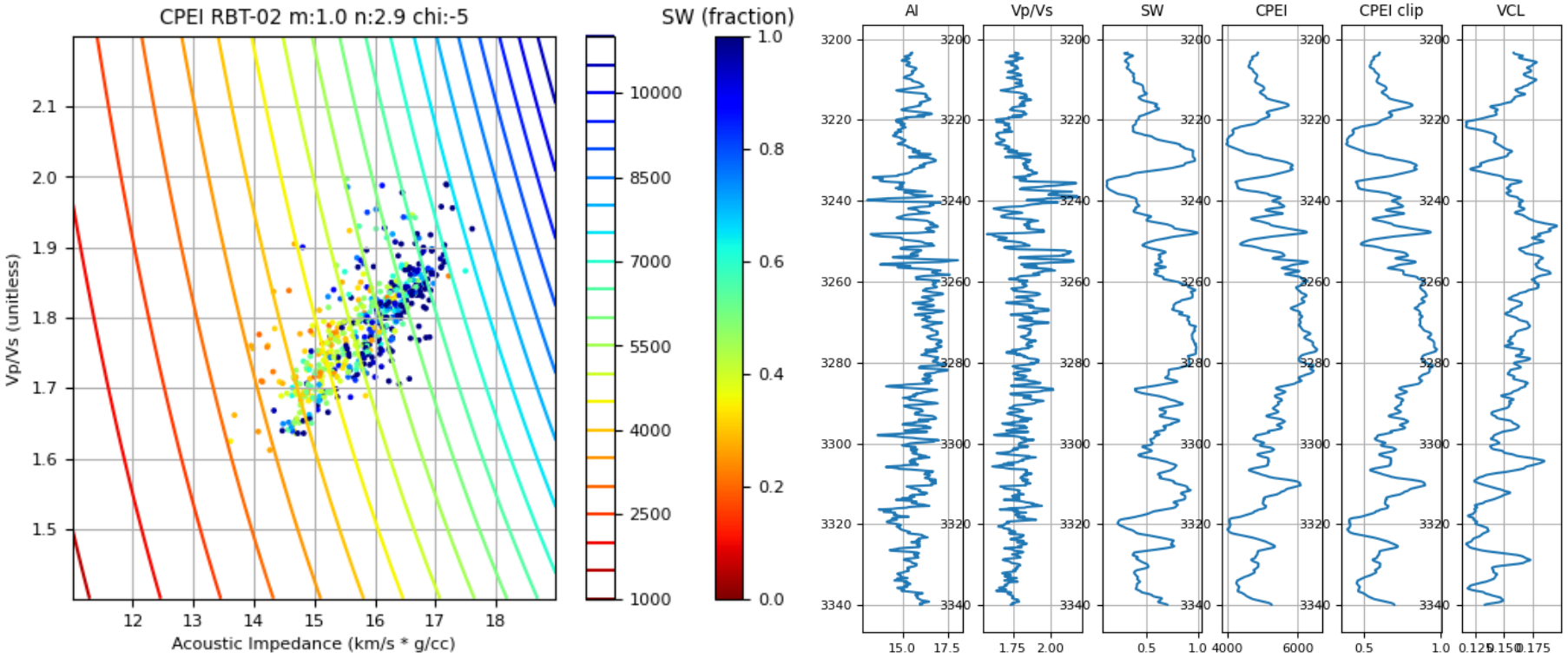

Figure 9. (Left) Calibrated CPEI attributes with respective well logs for the RBT-02 well. (Right) The CPEI-scaled attributes successfully approached the observed S_w logs.

 | DOI.org/10.29017/scog.v48i1.1686

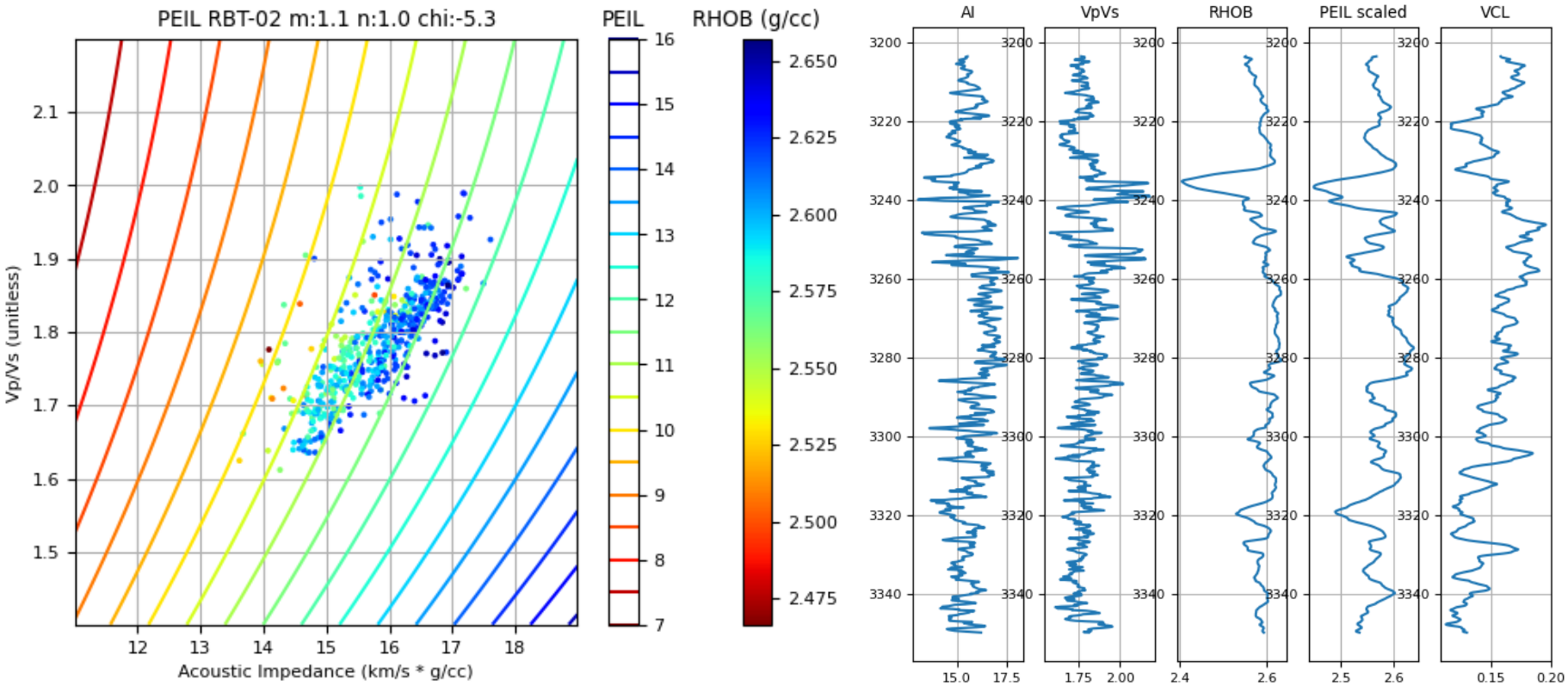

Figure 10. (Left) Calibrated PEIL attributes with respective well logs for the RBT-02 well. (Right) The PEIL attribute successfully approached the observed RHOB log value.

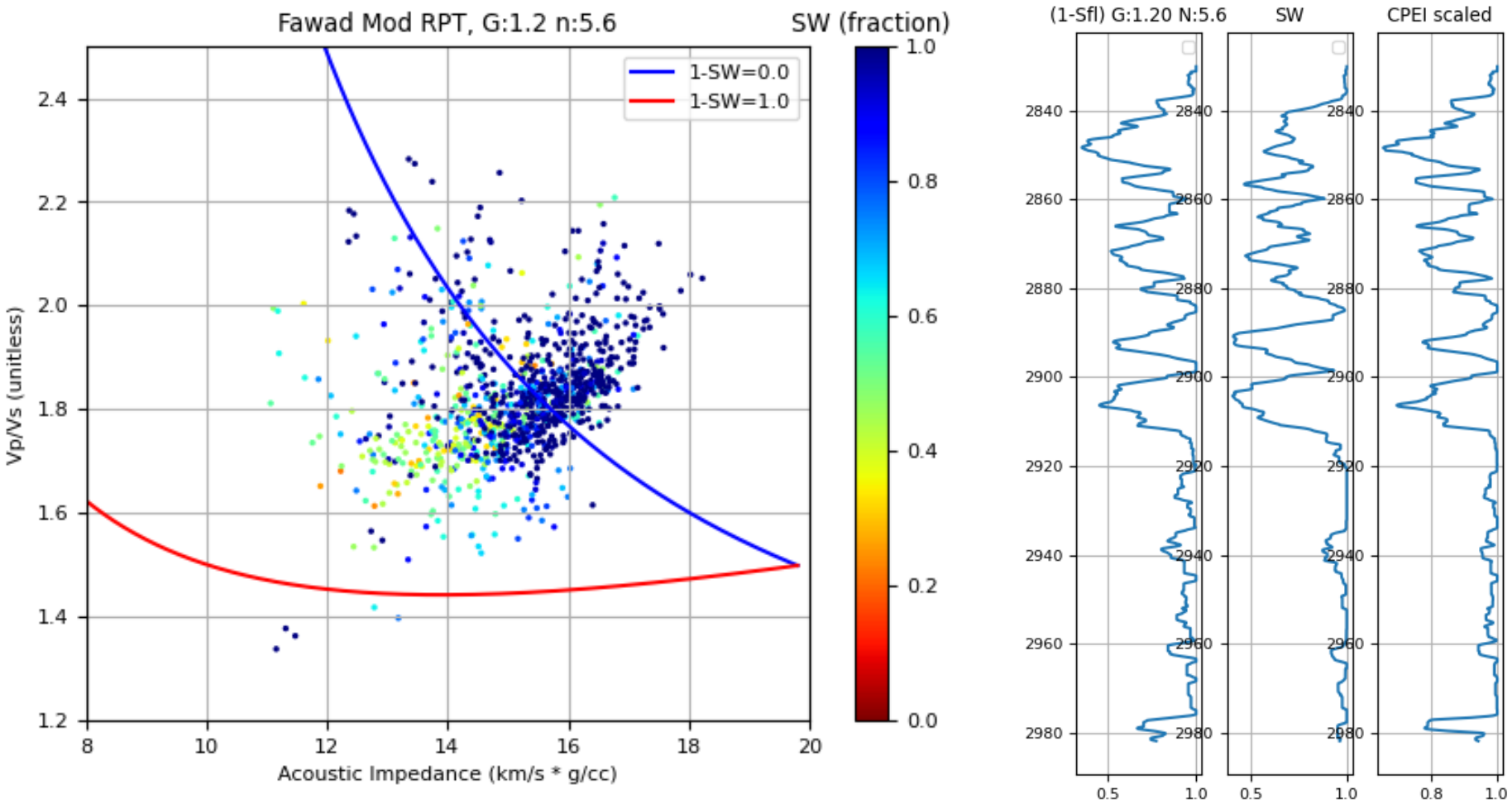

Figure 11. (Left) The RPT shows the distribution of AI and *Vp/Vs* with the color key depicting the water saturation log for the KTB-02 well. (Right) Estimated fluid saturation with the S_w log and CPEI attributes.

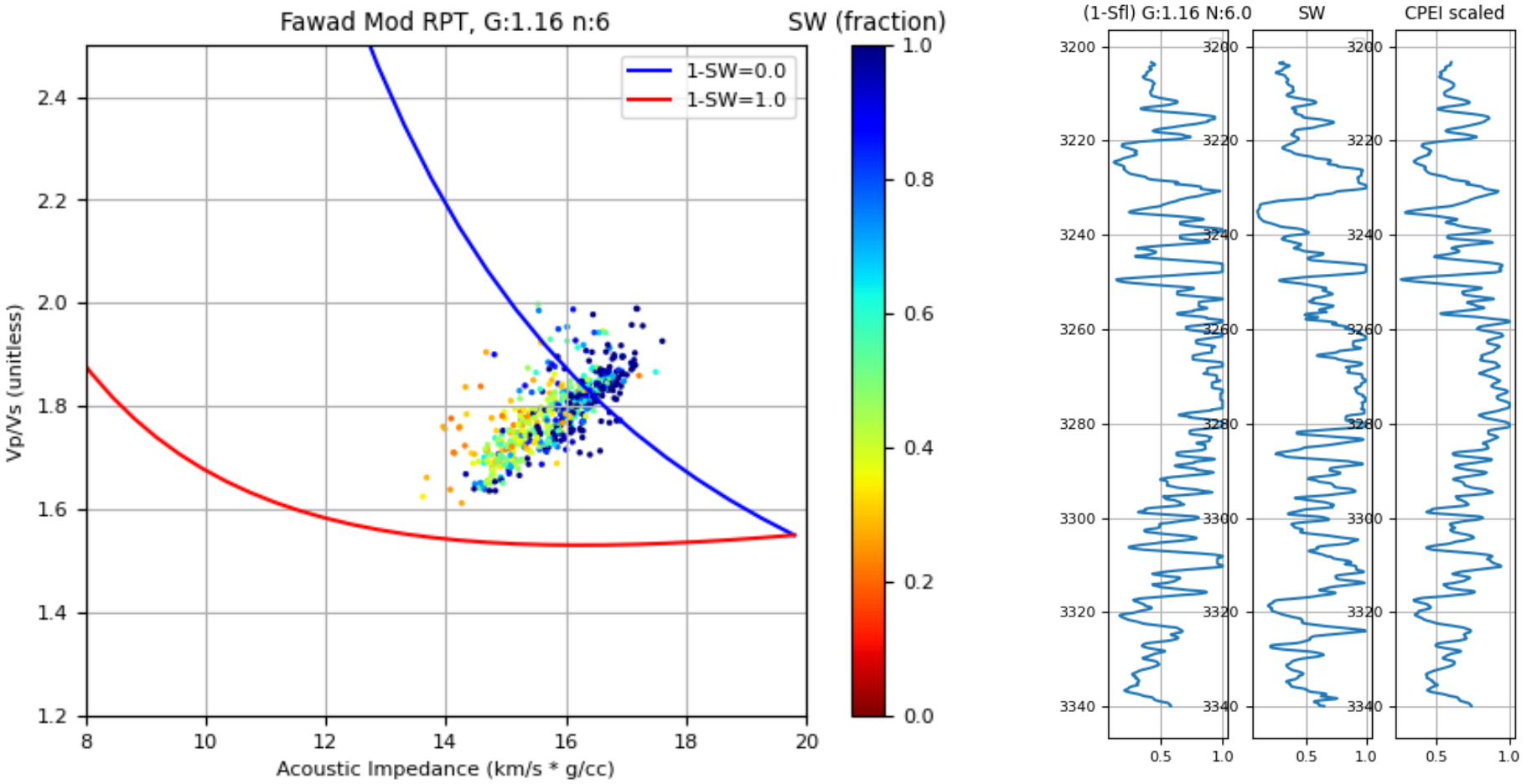

Figure 12. (Left) The RPT shows the distribution of AI and *Vp/Vs* with the color key depicting the water saturation log for the RBT-02 well. (Right) Estimated fluid saturation with the S_w log and CPEI attributes.

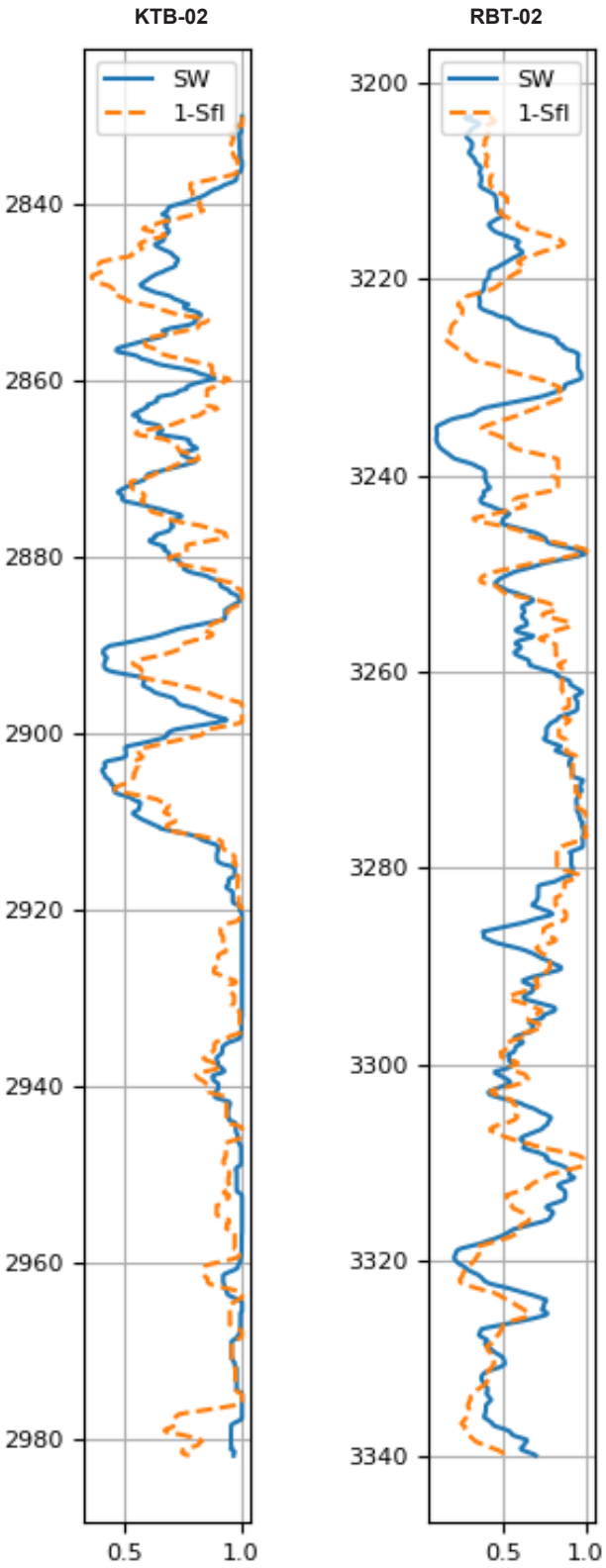

Figure 13. Water saturation estimation (1-*Sfl*) using the proposed MFM-RPT model (Orange dashed line) compared with the observed water saturation log (Blue solid line), showing similar trends and values.

Currently, the method used in this study is applied only to well data. Application to inverted seismic data still needs to be carried out in the future to further test the proposed model on seismic data. Because the proposed workflow utilizes the CPEI and PEIL attributes to calibrate the model, the process and cost of computation are longer. The calibration process of model parameters *G* and *N* directly to the well data; e.g., the water saturation log, needs to be investigated in the future to further simplify the process and save computation time. The remaining misfit between the observed water saturation log and the predicted fluid saturation can be improved by performing iterations on the fluid/hydrocarbon parameter; i.e., apparent velocity and density, until it is well aligned with the water saturation log. Fluid-mixing models; (i.e., patchy saturation between CO_2 and brine, can also be employed to improve the fitting of fluid saturation. Considering the clay content in the reservoir rock can also be beneficial for improving the porosity value estimation, thus improving the fluid saturation prediction.

CONCLUSION

The results show that the proposed workflow and method can predict water saturation in reservoir rocks using a novel approach that does not require modeling the elastic moduli of rock minerals, yet still allows calibration to the available data. The observed trend in the theoretical curve indicates that the proposed model better accommodates the porosity and fluid saturation trends in the AI and *Vp/Vs* model space compared to the original model. The proposed method also provides a very good estimation of water/fluid saturation, as indicated by the high cross-correlation and low misfit value between the calculated result and the observed water saturation log.

ACKNOWLEDGEMENT

The authors acknowledge SATREPS for their financial assistance and technical support for this research. The authors are also grateful to the Indonesia Endowment Fund for Education (LPDP) under the Ministry of Finance, Republic of Indonesia for providing a scholarship and supporting this study. Additionally, the authors thank the Center for CO_2 and Flared Gas Utilization at Institut Teknologi Bandung for their funding contributions, as well as Pertamina for granting permission and providing field data.

Symbol	Definition	Unit
AI	Acoustic Impedance	
CCS	Carbon Capture and Storage	
CPEI	Curved Pseudo Elastic Impedance	
EGR	Enhanced Gas Recovery	
FM-RPT	Fawad Mondol Rock Physics Template	
MFM-RPT	Modified Fawad-Mondol Rock Physics Template	
PEIL	Pseudo Elastic Impedance for Lithology	
RHOB	Rock's Bulk Density	g/cc
RPT	Rock Physics Template	
SATREPS	Science and Technology Research Partnership for sustainable Development	
Sw	Saturation of water	%
Sfl	Saturation of fluid	%
Vp	Velocity of P-wave	km/s
Vp_{ma}	P-wave velocity of rock matrix	km/s
	P-wave	

Vp_{fl}	velocity of fluid	km/s
Vs	Velocity of S-wave	km/s
Vs_{ma}	S-wave velocity of rock matrix	km/s

GLOSSARY OF TERMS

REFERENCES

Avseth, P., Mukerji, T., Mavko, G., & Dvorkin, J., 2010, Rock-physics diagnostics of depositional texture, diagenetic alterations, and reservoir heterogeneity in high-porosity siliciclastic sediments and rocks A review of selected models and suggested work flows. GEOPHYSICS 75, 75A31-75A47. https://doi.org/10.1190/1.3483770.

Avseth, P., Veggeland, T., & Horn, F., 2014, Seismic screening for hydrocarbon prospects using rock-physics attributes. The Leading Edge 33, 266–274. https://doi.org/10.1190/tle33030266.1

Avseth, P.A., Odegaard, E., 2004, Well log and seismic data analysis using rock physics templates. First Break 22. https://doi.org/10.3997/1365-2397.2004017.

Aziz, P.A., Nurhandoko, B.E.B., Marhaendrajana, T., Siagian, U.W.R., & Ariadji, T., 2025. The Effect of CO_2 Brine Rock Interaction Towards Sand Onset Modelling in Dolomite Rich Sandstone: A Case Study in Air Benakat Formation, South Sumatera, Indonesia. Scientific Contributions Oil and Gas 47, 3rd Edition (2024), 341–360. https https://doi.org/10.29017/SCOG.47.3.1682.

Aziz, P.A., Rachmat, M., Chandra, S., Daton, W.N., & Tony, B., 2023, Techno-Economic Solution For Extending Ccus Application In Natural Gas Fields: A Case Study Of B Gas Field In Indonesia. Scientific Contributions Oil and Gas 46, 1st Edition (2024), 19–28. https://doi.org/10.29017/SCOG.46.1.1321.

Batzle, M., & Wang, Z., 1992, Seismic properties of pore fluids. GEOPHYSICS 57, 1396–1408. https://doi.org/10.1190/1.1443207.

Crain, D.M., Benson, S.M., Saltzer, S.D., & Durlofsky, L.J., 2024, An integrated framework for optimal monitoring and history matching in CO$$_{2}$$ storage projects. Comput Geosci 28, 211–225. https://doi.org/10.1007/s10596-023-10216-3.

Fawad, M., & Mondol, N.H., 2022, Monitoring geological storage of CO2 using a new rock physics model. Sci Rep 12, 297. https://doi.org/10.1038/s41598-021-04400-7.

Fawad, M., & Mondol, N.H., 2021, Monitoring geological storage of CO_2: a new approach. Sci Rep 11, 5942. https://doi.org/10.1038/s41598-021-85346-8.

Gassmann, F., 1951, Elastic Waves Through A Packing of Spheres. GeophysicS 16, 673–685. https://doi.org/10.1190/1.1437718.

Gaus, I., 2010, Role and impact of CO_2–rock interactions during CO_2 storage in sedimentary rocks. International Journal of Greenhouse Gas Control 4, 73–89. https://doi.org/10.1016/j.ijggc.2009.09.015.

Hashin, Z., Shtrikman, S., 1963, A variational approach to the theory of the elastic behaviour of multiphase materials. J Mech Phys Solids 11, 127–140. https://doi.org/10.1016/0022-5096(63)90060-7.

Hutami, H.Y., Priniarti, T.L., Winardhi, I.S., . H., 2019. Rock Physics Template to Estimate The Effects of total Organic Carbon (TOC) and Mineralogy on The Seismic Elastic Properties of Immature Shale Reservoir. Scientific Contributions Oil and Gas 42, 43–49. https://doi.org/10.29017/SCOG.42.2.374.

IPCC, 2005, Carbon Dioxide Capture and Storage.

Lee, M.W., 2003. Velocity ratio and its application to predicting velocities. https://doi.org/10.3133/b2197.

Lee, M.W., Hutchinson, D.R., Collett, T.S., & Dillon, W.P., 1996. Seismic velocities for hydrate-bearing sediments using weighted equation. J Geophys Res Solid Earth 101, 20347–20358. https://doi.org/10.1029/96JB01886.

Luquot, L., Gouze, P., 2009, Experimental determination of porosity and permeability

changes induced by injection of CO_2 into carbonate rocks. Chem Geol 265, 148–159. https://doi.org/10.1016/j.chemgeo.2009.03.028.

Mindlin, R.D., 1949. Compliance of Elastic Bodies in Contact. J Appl Mech 16, 259–268. https://doi.org/10.1115/1.4009973.

Nugroho, D., Rudyawan, A., & Syihab, Z., 2023. Cenozoic Carbonate Reservoir in Indonesia Volume 1 : Unpublished Report, 1st ed, SKK Migas Memoir #2. ITB Press, Bandung.

Palgunadi, K.H., Viantini, I., Yogi, S., & Winardhie, S., 2016. A novel approach comparison of curved pseudoelastic impedance in rock physics analysis, in: SEG Technical Program Expanded Abstracts 2016. Society of Exploration Geophysicists, pp. 3448–3452. https://doi.org/10.1190/segam2016-13850446.1.

Pelemo-Daniels, D., Nwafor, B.O., Stewart, R.R., 2023. CO_2 Injection Monitoring: Enhancing Time-Lapse Seismic Inversion for Injected Volume Estimation in the Utsira Formation, Sleipner Field, North Sea. J Mar Sci Eng 11, 2275. https://doi.org/10.3390/jmse11122275.

Phani, K.K., Niyogi, S.K., 1986, Porosity dependence of ultrasonic velocity and elastic modulus in sintered uranium dioxide — a discussion. J Mater Sci Lett 5, 427–430. https://doi.org/10.1007/BF01672350.

Purwaningsih, M.E.M., Satyana, A.H., Budiyani, S., Noeradi, D., & Malik, N.M., 2002, Evolution of the Late Oligocene Kujung reef complex in the Western East Cepu High, East Java Basin: seismic sequence stratigraphic study. 31st IAGI Annual Conference.

Sule, M.R., Kadir, W.G.A., Matsuoka, T., Prabowo, H., & Sidemen, G.S., 2019, Gundih CCS Pilot Project: Current Status of the First Carbon Capture and Storage Project in South and Southeast Asia Regions. SSRN Electronic Journal. https://doi.org/10.2139/ssrn.3366415.

Winardhi, S., Dinanto, E., Sigalingging, A.S., Adityo, R., Utami, A.P., Ritonga, A.B., Satriawan, & W., Budiyono, 2023, Curved Pseudo Elastic Impedance based on Elastic Attribute Rotation Scheme for Reservoir Petrophysical Property Prediction. IOP Conf Ser Earth Environ Sci 1288, 012026. https://doi.org/10.1088/1755-1315/1288/1/012026.

Wyllie, M.R.J., Gregory, A.R., & Gardner, L.W., 1956. Elastic wave velocities in heterogeneous and porous media. GEOPHYSICS 21, 41–70. https://doi.org/10.1190/1.1438217.